Check for updates

Tracing carbon and nitrogen microbial assimilation in suspended particles in freshwaters

**Leonardo Mena-Rivera · Charlotte E. M. Lloyd ·
Michaela K. Reay · Tim Goodall · Daniel S. Read ·
Penny J. Johnes · Richard P. Evershed**

Abstract The dynamic interactions between dissolved organic matter (DOM) and particulate organic matter (POM) are central in nutrient cycling in freshwater ecosystems. However, the molecular-level mechanisms of such interactions are still poorly defined. Here, we study spatial differences in the chemical (i.e., individual proteinaceous amino acids) and microbial (i.e., 16S rRNA) composition of suspended sediments in the River Chew, UK. We then applied a compound-specific stable isotope probing (SIP) approach to test the potential assimilation of $^{13}C,^{15}N$-glutamate (Glu) and $^{15}N\text{-}NO_3^-$ into proteinaceous biomass by particle-associated microbial communities over a 72-h period. Our results demonstrate that the composition of suspended particles is strongly influenced by the effluent of sewage treatment works. Fluxes and percentages of assimilation of both isotopically labelled substrates into individual proteinaceous amino acids showed contrasting dynamics in processing at each site linked to primary biosynthetic metabolic pathways. Preferential assimilation of the organic molecule glutamate and evidence of its direct assimilation into newly synthesised biomass was obtained. Our approach provides quantitative molecular information on the mechanisms by which low molecular weight DOM is mineralised in the water column compared to an inorganic substrate. This is paramount for better understanding the processing and fate of organic matter in aquatic ecosystems.

Keywords Amino acids · Dissolved organic matter · Nitrate · Particulate organic matter · Stable isotope probing · Suspended particles

L. Mena-Rivera · C. E. M. Lloyd · M. K. Reay ·
R. P. Evershed (✉)
Organic Geochemistry Unit, School of Chemistry,
University of Bristol, Cantock's Close, Bristol BS8 1TS,
UK
e-mail: r.p.evershed@bristol.ac.uk

L. Mena-Rivera
School of Chemistry, Universidad Nacional,
Heredia 86-3000, Costa Rica

C. E. M. Lloyd · P. J. Johnes
School of Geographical Sciences, University of Bristol,
University Road, Bristol BS8 1SS, UK

T. Goodall · D. S. Read
UK Centre for Ecology & Hydrology (UKCEH),
Wallingford,, Oxfordshire 10 8BB, OX, UK

Introduction

The importance of organic matter in inland waters as nutrient and energy source for aquatic organisms (Mackay et al. 2020; Glibert et al. 2021), in controlling light attenuation (Mayer et al. 2006; Lu et al. 2013), and regulating the transport and

bioavailability of pollutants (Artifon et al. 2018) and metals (Yamashita and Jaffé 2008) is widely acknowledged. A significant amount of organic matter in freshwater is processed in transit to coastal areas or preserved in soils and sediments (Attermeyer et al. 2018). Organic matter partially contributes to the burial of 0.6 Pg of C yr^{-1} in freshwater sediments (Regnier et al. 2013) and to the evasion of 3.9 Pg of C yr^{-1} to the atmosphere (Drake et al. 2018), an amount equivalent to ~35% of the total anthropogenic CO_2 emissions. There is growing evidence that the concentration of organic matter has increased in freshwaters in the last decades (Evans et al. 2005; Monteith et al. 2007; Noacco et al. 2019). In this context, understanding the mechanisms in which organic matter, and related compounds, are processed across the landscape and within waterbodies is important to predict the potential impacts on the structure and functioning of the aquatic ecosystem.

Organic matter is typically classified as either dissolved (DOM) or particulate organic matter (POM) based on particle size with boundaries ranging from 0.2 to 0.7 µm. Although both phases exhibit different physical, chemical, and biological properties, they are actively linked to each other through several abiotic and biotic processes strongly influenced by environmental conditions (He et al. 2016; Einarsdóttir et al. 2020) including the degree of nutrient enrichment in the waterbody (Brailsford et al. 2019). Leaching and physical abrasion of POM contributes to the DOM pool (Yoshimura et al. 2010) while DOM can form POM via a range of physico-chemical processes including aggregation (Kerner et al. 2003), co-precipitation (Du et al. 2018) or selective sorption onto mineral surfaces (Aufdenkampe et al. 2001; Groeneveld et al. 2020). However, the processing of DOM is mainly regulated by living POM, whereby free-living and particle-associated microbial communities (Zeglin 2015; Mansour et al. 2018; Gweon et al. 2021) are central to the uptake of DOM into microbial organisms and primary producers, and its transfer to higher trophic levels.

Notably, particle-attached microbial communities are considered more active than their free-living counterparts (Crump et al. 1998; Smith et al. 2013). Suspended particles offer ecological conditions, such as light exposure and availability of nutrients, which enhance co-existence of microorganisms and population diversity (Nemergut et al. 2013).

Particle-attached microorganisms are therefore in a dynamic equilibrium with dissolved compounds, from which they can uptake nutrients. These biotic interactions that occur in the water column likely play a central role in nutrient cycling (Simon et al. 2002; Amalfitano et al. 2017; Glibert et al. 2021). Recently, Attermeyer et al. (2018) suggested that the partial loss of dissolved organic carbon (DOC) in rivers is due to remineralisation by suspended particle-attached microbes. Moreover, Jia et al. (2016) and Xia et al. (2017) showed that suspended particles impact nitrification and denitrification processes, expanding their significance to the processing of inorganic compounds (e.g., nitrate). It has been also demonstrated that particle-attached microorganisms respond to changes in nitrogen availability by potentially increasing assimilation (Bunch and Bernot 2012). Nevertheless, the molecular-level mechanisms by which these processes occur remain poorly defined.

Molecular-level and/or organism-specific processes can be elucidated through the application of stable isotope probing (SIP) techniques. SIP can provide metabolic and/or quantitative information relating to how a given isotopically enriched substrate is utilised by a complex microbial population. This is possible through the molecular analysis of labelled nucleic acids (DNA/RNA-SIP) (Manefield et al. 2002; Chen and Murrell 2010), the interpretation of images of biological samples via nano scale secondary ion mass spectroscopy (nanoSIMS) (Berthelot et al. 2019; Dekas et al. 2019) and Raman spectroscopy (Wang et al. 2016) or the isotopic analysis of specific biomarkers using gas chromatography-combustion-isotope ratio mass spectrometry (GC-C-IRMS) (Bull et al. 2000; Evershed et al. 2006). The latter has been successfully applied to study the incorporation of relevant substrates into microbial biomass in soils (Knowles et al. 2010; Charteris et al. 2016; Reay et al. 2019) and riverine benthic sediments (Veuger et al. 2005). Although stable isotopes have been widely used to study different biogeochemical processes in aquatic ecosystems [reviewed by Sánchez-Carrillo and Álvarez-Cobelas (2018)], most findings have relied on bulk isotopic measurements which limits the disentangling of molecular-level mechanisms.

Herein, we sought to investigate the mechanisms through which living suspended POM acts as a hot spot for the processing of DOM and related

compounds in a riverine ecosystem. We first studied the chemical and molecular composition of composite suspended particles collected at three sites in the River Chew, UK. We then conducted a SIP experiment where suspended particles were separately incubated with two isotopically enriched substrates under stable conditions. We used L-glutamic acid ($^{13}C,^{15}N$-Glu), a low molecular weight compound central in amino acid (AA) biosynthesis, and potassium nitrate (^{15}N-NO_3^-) that is one of the major nitrogen containing compounds in rivers and a pollutant of concern. We traced the assimilation of ^{13}C and/or ^{15}N via compound-specific isotope analysis of individual proteinaceous AAs using GC-C-IRMS. We hypothesised that organic and inorganic compounds, containing carbon and/or nitrogen, are partially assimilated into microbial biomass in the water column. We predicted a higher percentage of assimilation of the organic substrate in comparison to the inorganic substrate. We expected that the rates and magnitude of the isotopic enrichment (C and/or N) of individual AAs would provide information concerning the biochemical pathways by which the substrates are assimilated.

Materials and methods

Study site and sampling

River Chew is a lowland river located in Bath and Northeast Somerset, United Kingdom. It flows from Chew Valley Lake, south–west of Bath, to the north–east, where it discharges into the Bristol Avon near the town of Keynsham, which then flows west to the Bristol Channel. The catchment covers an area of 143 km^2. Discharge in the River Chew is highly influenced by the regime of water release from Chew Valley Lake, a man-made reservoir that supplies drinking water to the city of Bristol, as well as effluent discharges from a sewage treatment works (STW). The study area is designated a Special Protection Area (SPA) and Site of Special Scientific Interest (SSSI). The treatment methods at the STW comprises (a) removal of large materials, (b) a primary settlement stage for further reduction of particle load, (c) biological filters (mixture of stone and plastic media) for breakdown of organic matter, followed by a humus settlement tank, and (d) aerated tertiary sand filters for phosphorus removal. The STW discharge accounts for 20–50% of the total stream discharge.

Suspended particles were collected from three contrasting sites in the upper River Chew tributary (Fig. S1) using time-integrated sediment samplers (Phillips et al. 2000). These were located downstream of the reservoir (S1), at the effluent discharge point from the STW (S2), and downstream from the STW discharge (S3) where the stream was fully mixed under baseflow conditions. Samplers, one per site, were placed at 60% depth in the water column on a fixed frame from September 7th to October 12th, 2018. (Phillips et al. 2000). Weekly routine checks were carried out to minimise inlet and outlet clogging. The devices were sealed in the field and transported to the laboratory within 2 h. The sediments were extracted from each device and stored at 4 °C in in situ river water until further experiments; sub-samples for microbial community analysis were stored at −70 °C. In addition, 2 L of river water was extracted from each sampler, filtered using 0.5 µm pre-combusted (450 °C, 4 h) glass fibre filters (Advantec® GC-50, Japan) and stored at −20 °C. The filtered river water was used for nutrient analyses and for the SIP experiment.

Bulk measurements and nutrient analysis

Total carbon (TC) and total nitrogen (TN) of freeze-dried suspended particles were determined using a Thermo EA1110 elemental analyser (MA, USA). Bulk ^{13}C and ^{15}N isotopic determinations were determined using a Flash EA1112 Series NC Analyser coupled to a Thermo Finnigan DeltaPlus XP (MA, USA). Inorganic nutrient analyses on filtered river water were conducted using a Skalar San^{++} multi-channel continuous flow analyser (Breda, The Netherlands) following the procedures outline by (Yates et al. 2019). Nitrite (NO_2-N) was determined colourimetrically at 540 nm after the reaction with N-(1-naphthyl)ethylenediamine dihydrochloride. Total oxidised nitrogen ($TON = NO_2$-N$ + NO_3$-N) was determined using the same principle as nitrite analysis after nitrate reduction by hydrazinium sulfate. Nitrate concentrations were calculated by subtraction of NO_2-N from TON. Total ammonium (NH_3-N$ + NH_4$-N) analysis was based on the modified Berthelot reaction and measured at 660 nm. Soluble reactive phosphorus (PO_4-P)

was determined using the molybdate/ascorbic acid blue method and measured at 880 nm.

Microbial community analysis

DNA was extracted from suspended sediments using a PowerSoil® DNA Isolation Kit according to the manufacturer's instructions. Bacterial amplicons were generated using a 2-step amplification approach, with Illumina Nextera tagged primers: 16S rRNA (V4-V5 region) 515F GTGYCAGCMGCCGCGGTAA and 806R GGACTACNVGGGTWTCTAAT (Walters et al. 2016), each modified at 5′ end with the addition of Illumina pre-adapter and Nextera sequencing primer sequences. Amplicons were generated using a high-fidelity DNA polymerase (Q5 Taq, New England Biolabs). After an initial denaturation at 95 °C for 2 min, PCR conditions were: denaturation at 95 °C for 15 s; annealing at 50 °C. Annealing times were 30 s with extension at 72 °C for 30 s; repeated for 30 cycles. A final extension of 10 min at 72 °C was included. PCR products were purified using Zymo ZR-96 DNA Clean-up Kit following the manufacturer's instructions. MiSeq adapters and 8nt dual-indexing barcode sequences were added during a second step of PCR amplification. After an initial denaturation 95 °C for 2 min, PCR conditions were: denaturation at 95 °C for 15 s; annealing at 55 °C. Annealing times were 30 s with extension at 72 °C for 30 s; repeated for 8 cycles with a final extension of 10 min at 72 °C. Amplicon sizes were determined using an Agilent 2200 TapeStation system. Libraries were normalized using SequalPrep Normalization Plate Kit (Thermo Fisher Scientific) and quantified using Qubit dsDNA HS kit (Thermo Fisher Scientific). Each amplicon's pooled library was diluted to achieve 400 pM with 7.5% Illumina PhiX. Denaturation of each library was achieved with addition of 10% final volume of 2 M NaOH for 5 min followed by neutralisation with an equal volume of 2 M HCl. The libraries were then diluted to their load concentrations with Illumina HT1 Buffer. A final denaturation was performed by heating the libraries to 96 °C for 2 min followed by cooling in crushed ice. Sequencing of each amplicon library was performed on Illumina MiSeq using V3 600 cycle reagents.

SIP experiment

Mesocosms consisted of 300 mg of suspended sediments (wet weight) in 450 mL of in situ sterile-filtered river water. The latter was re-filtered and autoclaved (121 °C, 15 psi, 30 min) on the day of the experiment. In situ river water was used in the mesocosms to keep experimental and natural nutrient concentrations close to in situ, given the known impact of nutrient enrichment on organic matter processing in streams (Brailsford et al. 2019). The SIP experiment was carried out within 3 days of sample' collection. Experiments were conducted in 1 L pre-combusted Duran® bottles (450 °C, 4 h) at 19 °C and under fluorescent light; constant-gentle stirring was applied to minimise sedimentation. An overnight acclimatisation period was allowed prior to substrate addition. Two treatments (L-glutamic acid and KNO_3) and a control were set up per site. Incubations were started after the addition of 100 μL of 25 mM L-glutamic acid ($x(^{13}C) = 99\%$, $x(^{15}N) = 99\%$); Sigma Aldrich) or 100 μL of 320 mM KNO_3 [$x(^{15}N) = 10\%$; Sigma Aldrich]. Isotopes were added to increase the $\delta\,^{15}N$-value in the river water by ~10,000 ‰, which resulted in an increase of ~1 mg/L N. Each mesocosm was sampled twice (2×50 mL) after 3, 24, 48 and 72 h. Aliquots were immediately filtered using 0.5 μm pre-combusted (450 °C, 4 h) glass fibre filters (Advantec® GC-50, Japan); the latter were rinsed twice with double distilled water to remove the excess of substrate. Both fractions sampled (sediments and filtered river water) were then stored at −20 °C.

Total hydrolysable amino acids

The concentration of total hydrolysable amino acids (THAAs) was determined following Charteris et al. (2016). In brief, freeze-dried sediments (~10 mg) were hydrolysed with 5 mL of 6 M HCl at 100 °C for 24 h under N_2. An internal standard (norleucine, 1000 μg mL^{-1}) was added before hydrolysis. Hydrolysates were separated by centrifugation, dried under N_2 at 60 °C and stored in 0.1 M HCl at −20 °C until further analysis. AAs were isolated by cation-exchange column chromatography (Dowex® 50WX8) and converted into their N-acetyl, O-isopropyl derivatives with acetyl chloride, trimethylamine, and acetic anhydride. Derivatives were then quantified by conventional gas chromatography (GC-FID)

(Agilent Technologies 7890B, CA, USA). The system was fitted with a DB-35 column (35%-phenyl-methylpolysixane, mid-polarity, 30 m×0.32 mm inner diameter, film 0.5 μm). The carrier gas was He at 2 mL min^{-1} and the GC operated under constant flow. The temperature programme used was: 70 °C (2 min) to 150 °C at 15 °C min^{-1}, then to 210 °C at 2 °C min^{-1}, then to 270 °C (10 min) at 8 °C min^{-1}. Quantification of individual AAs was based on the internal standard method and individual response factors for each AA.

GC-C-IRMS analysis

The ^{13}C and ^{15}N values of the individual derivatised AAs were determined via GC-C-IRMS. ^{15}N determinations were performed using a Thermo Finnigan Trace 2000 GC (Milan, Italy) coupled with a Thermo Finnigan DeltaPlus XP IRMS (Bremen, Germany) via a GC Combustion III interface. The GC was fitted with a DB-35 column (35%-phenyl-methylpolysiloxane, mid-polarity, 30 m×0.32 mm inner diameter, film 0.5 μm). The temperature programme was: 40 °C (5 min) to 120 °C at 15 °C min^{-1}, then to 180 °C at 3 °C min^{-1}, then to 210 °C at 1.5 °C min^{-1}, then to 270 °C (1 min) at 5 °C min^{-1}. The carrier gas was He at 1.4 mL min^{-1} and the GC operated in constant flow mode. Individual derivatised AA were combusted at 1030 °C over Cu and Ni wires. A cryogenic trap with liquid nitrogen was used to remove CO_2. The mass spectrometer was operated in EI mode at 124 eV and data acquisition included m/z 28, 29 and 30. Carbon isotopic determinations were carried out using a Trace GC Ultra (Bremen, Germany) coupled with a Thermo Finnigan Delta V (Bremen, Germany) IRMS. The GC was operated under the same conditions described for the ^{15}N measurements, except for the carrier gas flow which was set at 1 mL min^{-1}. The reactor temperature was 1000 °C. The mass spectrometer was operated in EI mode at 124 eV and data acquisition included m/z 44, 45 and 46. The original δ ^{13}C value of each individual AAs was determined after correction of its derivatised form (Docherty et al. 2001).

Data analysis

All data processing was performed in R version 4.1.0 (R Core Team 2021).

Bioinformatics

Each amplicon's Illumina demultiplexed sequences were processed using packages *ShortRead* (Morgan et al. 2009) and *Biostrings* (Pagès et al. 2021), along with cutadapt (Martin 2011) to search for and remove primers. DADA2 (Callahan et al. 2016) was used to filter, denoise and merge the sequences with the following parameters: forward reads were trimmed to 250 bp and reverse to 200 bp. Filtering settings were maximum number of sequences containing unassigned bases (Ns) (maxN)=0, maximum number of expected errors (maxEE)=(5,5). Sequences were de-replicated and the DADA2 core sequence variant inference algorithm applied. Forward and reverse reads were then merged using the merge Pairs function to produce Amplicon sequence variants (ASVs). Chimeric sequences were removed using remove Bimera Denovo at default settings and the sequence table constructed from the resultant ASVs. ASVs were subject to taxonomic assignment using assign Taxonomy function and the SILVA training database (Quast et al. 2013).

SIP calculations

Isotopic enrichments of individual AAs are reported as the normalised excess atom fraction following:

$$x^E(^iE)_N = \frac{x(^iE)_P - x(^iE)_c}{x(^iE)_s}$$

where $x^E(^iE)_N$ is the normalised excess atom fraction of the isotope ^iE (^{13}C or ^{15}N) of an individual AA, $x(^iE)$ is the atom fraction of the enriched isotope in that AA in the sample (P) or the control (c), and $x(^iE)_s$ is the atom fraction of the isotope in the substrate corrected for any dilution effect due to background/ambient concentration. The atom fractions are calculated from the δ-value (Coplen 2011) following:

$$x(^iE) = \frac{1}{1 + \frac{1}{(\delta^iE+1)R(^iE/^jE)_{std}}}$$

where $R(^iE/^jE)_{std}$ is the heavy to light isotope ratio of internationally agreed standards. Stable isotope standards include the Vienna Pee DeeBelemnite (VPDB) (^{13}C/^{12}C=0.011180) (Brand et al. 2010) and air

(^{15}N/^{14}N$=0.0112372$) (Junk and Svec 1958; Meija et al. 2016) for C and N determinations, respectively.

Specific assimilation (V) and transport rates (ρ) for each AA were calculated after 3 h (Dugdale and Goering 1967; Glibert et al. 2019). Enrichments are also reported as the percentage of assimilation, $A(^iE)_{AA}$, into each individual AA derived from the added substrate (Knowles et al. 2010) following:

$$A(^iE)_{AA} = \frac{mol^E(^iE)_P}{mol(^iE)_s}100$$

where $mol^E(^iE)_P$ is the total amount of the enriched isotope (^{13}C or ^{15}N) in the mesocosm, and $mol(^iE)_s$ is the amount of that isotope added from the substrate. Negligible losses of the substrate over time are assumed.

Statistical analysis

Linear mixed-effects modelling was applied to evaluate the significance of sampling location, treatment, and incubation period (i.e., time) in explaining the variation of the concentration of THAAs, or individual AAs, during the SIP experiment. Sampling location, treatment, and time were set as fixed effects, and the mesocosms as a random effect. Assumptions of normality and homoscedasticity were checked using standard diagnostics graphs. Final model selection was based on the Akaike Information Criterion (AIC). Models were run using the *nlme* package (Pinheiro et al. 2021).

Deming regression was applied to estimate the ^{13}C:^{15}N ratio of Glx (Glu + Gln) and Pro during the first 24 h of incubation. The correlation coefficient between ^{13}C and ^{15}N for each AA was calculated using Spearman's rank correlation. Significant differences between the ^{13}C:^{15}N ratio of Glx and Pro were tested by contrasting the regression slopes using a *t*-test.

Results and discussion

Chemical composition of suspended particles

Differences in the chemical composition of the suspended particles in the River Chew, UK were observed between sites (Table 1). The impact of the

Table 1 Summary of the composition of suspended POM in the River Chew, UK

Parameter	Site		
	S1	S2	S3
Bulk			
TC (%)	5.45	9.96	5.32
TN (%)	0.62	1.34	0.65
C:N ratio	8.82	7.47	8.20
δ^{13}C (‰)	−23.41	−26.75	−26.19
δ^{15}N (‰)	10.78	14.17	12.78
Amino acids (mg g^{-1})			
Ala	2.55	6.09	2.27
Asx	4.92	12.04	4.73
Glx	3.68	9.31	4.06
Gly	2.58	6.24	2.44
Hyp	0.43	0.76	0.45
Leu	2.36	5.06	2.38
Lys	1.14	3.12	1.05
Phe	0.70	1.66	0.66
Pro	1.54	3.64	1.66
Ser	2.81	7.05	2.69
Thr	3.32	8.01	3.18
Tyr	0.40	0.93	0.14
Val	1.72	4.00	1.64
THAAs (mg g^{-1})	28.14	67.92	27.34
THAAs-C of TC (%)	13.2	17.3	14.2
THAAs-N of TN (%)	56.7	63.5	52.2
16S rRNA gene sequencing			
Number ASVs	646	571	399
Shannon index	5.39	5.28	4.88

Asx aspartic acid + asparagine, *Glx* glutamic acid + glutamine

STW effluent led to an increase in the concentration of TC, TN and THAAs. In addition, bulk δ^{15}N values showed enrichment (~3%) at sites S2 and S3, which has been previously associated with human sewage pollution (Steffy and Kilham 2004; Costanzo et al. 2005). A total of 13 AAs were identified with concentrations ranged from 0.40 to 4.92 mg g^{-1} at site S1, from 0.76 to 12.04 mg g^{-1} at site S2, and from 0.14 to 4.73 mg g^{-1} at site S3. The contribution of the THAAs to the TC and to the TN accounted for $> 10\%$ and $> 50\%$, respectively. The molecular composition of the pool of THAAs, expressed as mol %, followed: Asx (Asp + Asn) > Gly > Ala > Thr > Ser > Glx > Leu > Val > Pro > Lys > Phe > Hyp > Tyr. This overall composition agrees with previous studies where

the neutral, acidic and hydroxyl AAs were reported to be the most dominant (Gupta et al. 1997; Fernandes et al. 2019, 2020). The high contribution of the THAAs to TN and the relatively moderate abundance of Gly (~14%) indicate the high bioavailability and low diagenetic state of organic matter in the suspended sediments (Cowie and Hedges 1994; Dauwe and Middelburg 1998). The decrease in the concentration of individual AAs at site S3 might suggest a different source of suspended particles; however, similarities in the δ ^{15}N values of individual AAs shows connectivity in the transport of suspended particles between sites S2 and S3 (Table S1). Therefore, the composition of the suspended material at site S3 appears to be a mixture of particles from the STW outfall with contribution from the floodplains or bank erosion at this site.

Microbial community composition

High throughput sequencing revealed changes in the diversity and composition of the riverine microbial communities upstream and downstream from the STW effluent discharge point. In total 147,425 high-quality bacterial 16S rRNA gene sequences were obtained and classified into 1111 ASVs. Both richness and diversity decreased downstream from the STW effluent (Table 1). This phenomenon has been previously observed in freshwaters receiving sewage effluents (Drury et al. 2013; Burdon et al. 2020). Although treated and untreated sewage discharges are known to increase the bioavailability of both dissolved organic and inorganic nitrogen and phosphorus in freshwaters (Yates et al. 2019) stimulating bacterioplankton growth, the discharge of potentially harmful compounds that escape conventional treatment could explain the negative impact on microbial diversity (Chonova et al. 2018; Hagberg et al. 2021). In the same study reach, Pemberton et al. (2020) reported changes in the chemical composition of DOM due to STW effluent, highlighting the presence of pharmaceuticals, illicit drugs, and flame retardants. Future studies are needed to assess the impact of these pollutants on the structure and functioning of aquatic microorganism communities. Despite the observed decrease in diversity, the three sampling sites shared 159 ASVs which comprised for 55.7–64.0% of the total relative abundance. Adjacent sites shared higher number of ASVs. For instance, site S1 and S2 shared
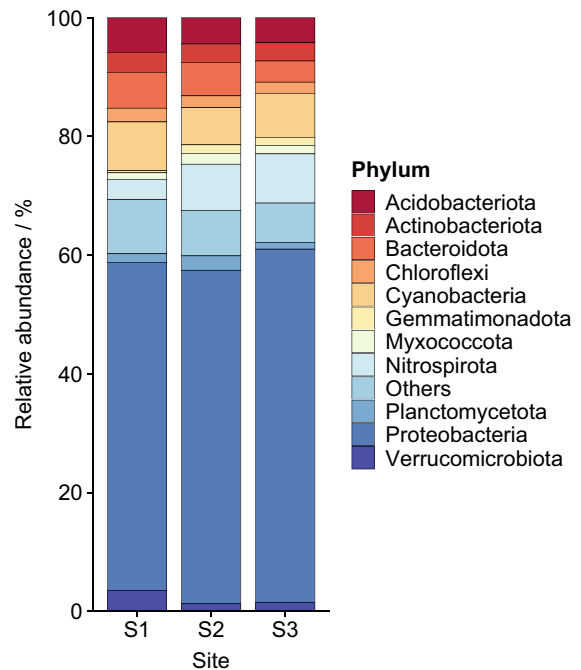

Fig. 1 Phylum level bacterial community composition in suspended POM in the River Chew, UK based on 16S rRNA gene sequencing

84 additional ASVs (243 in total), whereas sites S2 and S3 shared 63 ASVs (222 in total).

The composition of the microbial communities associated with the suspended particles was dominated by *Proteobacteria* (55.3–59.5%) (Fig. 1); in particular, the class *Gammaproteobacteria* was the most abundant as found in other riverine sediments (Wang et al. 2018). Less abundant phyla were *Cyanobacteria* (6.3–8.2%), *Nitrospirota* (3.3–8.3%), *Bacteroidota* (3.6–6%), and *Acidobacteriota* (4.2–5.9%). Among the three sites, the shared ASVs included the phyla described in Fig. 1, together with *Desulfobacterota*, *NB1-j* and *RCP2-54*, which were found in <1% of the relative abundance. Some spatial differences in microbial composition were also observed. The relative abundance of *Proteobacteria* and *Nitrospirota* increased downstream (>4%), whereas the relative abundance of *Bacteroidota* and *Acidobacteriota* decreased (<3%). The phyla *WPS-2* and some classes such as *OLB14*, *TK10*, *Babeliae*, *Gracilibacteria*, *Kapabacteria* and *Vampirivibrionia* were only found at sites S2 and S3. The higher abundance of *Proteobacteria* downstream (sites S2 and S3) might be

related to the increase in the concentration of nutrients in the stream due to the STW effluent. This is in line with previous studies showing a positive correlation between the abundance of *Proteobacteria* and the availability of nutrients (Dai et al. 2013). Similarly, *Nitrospirota* are abundant in STW and well known for catalysing the second step of nitrification (Wu et al. 2019); thus, their increased abundance may be a result of an increase in the concentration of ammonium in the stream. In general, the microbial composition mainly comprised of heterotrophic organisms with the potential ability to degrade a broad range of organic compounds. Estimating the fluxes in the processing of these organic compounds compared to inorganic compounds, at different spatial and temporal scales, is key to understanding the biogeochemical cycling.

SIP experiment

THAAs concentration

The results of the mixed effects model showed that the addition of the two isotopically enriched substrates had a negligible effect on the concentration of THAAs in the suspended particles during the SIP experiment $[F(2,4) = 3.44, P = 0.135]$. The observed changes were associated with the sampling location (i.e., site) $[F(2,4) = 74.78, P = 0.0007]$ and time $[F(1,62) = 21.62, P < 0.0001]$ (Fig. S2). The effect of site confirmed that the concentration of THAAs in the suspended particles was higher at site S2 in comparison to sites S1 and S3, as shown in section "Chemical composition of suspended particles". During the incubation period, the standard error and the confidence interval of the means per site were 1.4 and 7.7 mg g^{-1} (95% confidence level), respectively.

Because one of the added substrates was Glu, and sorption processes of AAs onto sediments have been previously reported (Aufdenkampe et al. 2001; Hunter et al. 2016), the variation in the concentration of Glx was also tested. Similar results to the concentration of THAAs were obtained. The effects of sampling location $[F(2,4) = 37.59, P = 0.0026]$ and time $[F(1,62) = 25.36, P < 0.0001]$ were related to the changes in the concentration of Glx. The effect of treatment was also likely significant $[F(2,4) = 6.88, P = 0.0507]$. However, the slightly higher concentrations of Glx were only observed in the controls. These results indicate that sorption processes of $^{13}C,^{15}N$-Glu onto the mineral phase or biomass on the particles were likely negligible, suggesting that the $^{13}C,^{15}N$-Glu measured in excess was primarily taken up into microbial cells.

$^{13}C,^{15}N$-Glu treatment

Isotope values of individual AAs showed transfer of ^{13}C and ^{15}N from Glu into newly synthesised protein biomass. This isotopic enrichment was used to estimate specific assimilation rates (V, h^{-1}) for each AA. Assimilation rates of ^{15}N were higher than ^{13}C (Table S2). The assimilation of ^{15}N from Glu is expected to be faster as it participates in single-step transamination reactions in the biosynthesis of other AAs (Knowles et al. 2010). On the other hand, the assimilation of ^{13}C is mediated by glutamate dehydrogenase where Glu is first deaminated to produce ammonium and 2-oxoglutarate. The latter is then incorporated into the citric acid cycle (TCA) (Miflin and Habash 2002; Feehily and Karatzas 2013). Lys and Asx showed the highest average assimilation rates for both isotopes. In contrast, Hyp and Leu showed the lowest average assimilation of ^{13}C and ^{15}N, respectively. It should be noted that the low concentration of Hyp and Tyr impeded determination of their ^{15}N contents.

A quantitative assessment of the assimilation of both isotopes, as given by the estimation of transport rates (nmol g^{-1} h^{-1}), showed higher assimilation of ^{13}C over ^{15}N, except for Gly (Table S3). The highest average values were presented in Asx, which is in close metabolic proximity to Glu, but also in high abundance. The higher transport of ^{15}N over ^{13}C into Gly during the first 3 h of incubation is particularly interesting as it might suggest that the main biosynthetic pathway of Gly was not dominant. Gly is primarily biosynthesised from Ser; in this pathway, 3-phosphoglycerate is oxidised to 3-phosphohydroxypiruvate followed by the addition of an amino group by a 3-phosphoserine aminotransferase to produce 3-phosphoserine. The latter is then hydrolysed to form Ser, which can be converted to Gly by serine hydroxymethyltransferase (Stauffer 2004). A significantly fast transamination reaction followed by the conversion of Ser to Gly could explain the higher assimilation of ^{15}N over ^{13}C. However, transport

rates of ^{15}N into Ser do not fully support this as they were lower compared to those of Gly. Gly can also be biosynthesised from glyoxylate (Conley et al. 2017; Caspi et al. 2019). In this case, the transamination is mediated by alanine. If this pathway was dominant, it could explain the high incorporation of ^{15}N into Gly. The faster assimilation and high transport rates of ^{15}N into Ala versus Gly support this hypothesis.

Based on the amount of substrate added, the percentage of assimilation of ^{15}N was higher than ^{13}C, except in Phe (Fig. 2). In most cases, the decoupling between both isotopes likely occurred after 3 h of incubation. However, this was not the case for Glx and Pro where the coupling was conserved up to 24 h after the substrate addition. Trends in assimilation were different among AAs, but they were likely linear during the first 24 h of the experiment. After this period, some AAs, such as Ala, Gly, Leu, and Phe, likely reached a plateau or showed an apparently decreasing trend. In contrast, Ser, Thr and Val

showed an increasing trend of assimilation over the course of the experiment. Unlike the other AAs, Lys showed an exponential assimilation. After 72 h, average microbial assimilation of ^{13}C was dominated by Glx ($M=2.91\%$, $SE=0.13$) and Asx ($M=2.22\%$, $SE=0.11$) while the assimilation of ^{15}N was higher in Asx ($M=4.70\%$, $SE=0.22$), Glx ($M=4.19\%$, $SE=0.22$), Gly ($M=4.03\%$, $SE=0.32$) and Ala ($M=3.92\%$, $SE=0.43$). Microbial assimilation of Glx included in excess ^{13}C,^{15}N-Glu.

To better understand the uncoupling of ^{13}C and ^{15}N, the ^{13}C:^{15}N ratio was estimated for all the individual AAs at each time point (Fig. 3A). After 3 h of incubation, two maximum values were observed, corresponding to ^{13}C:^{15}N ratios of nearly two and five. As expected, the ratio shifted towards lower values over time. This is likely due to the transfer of ^{13}C into the biosynthesis of non-proteinaceous compounds or its release as CO_2; for instance, during the conversion of 2-oxoglutarate into succinyl-CoA.
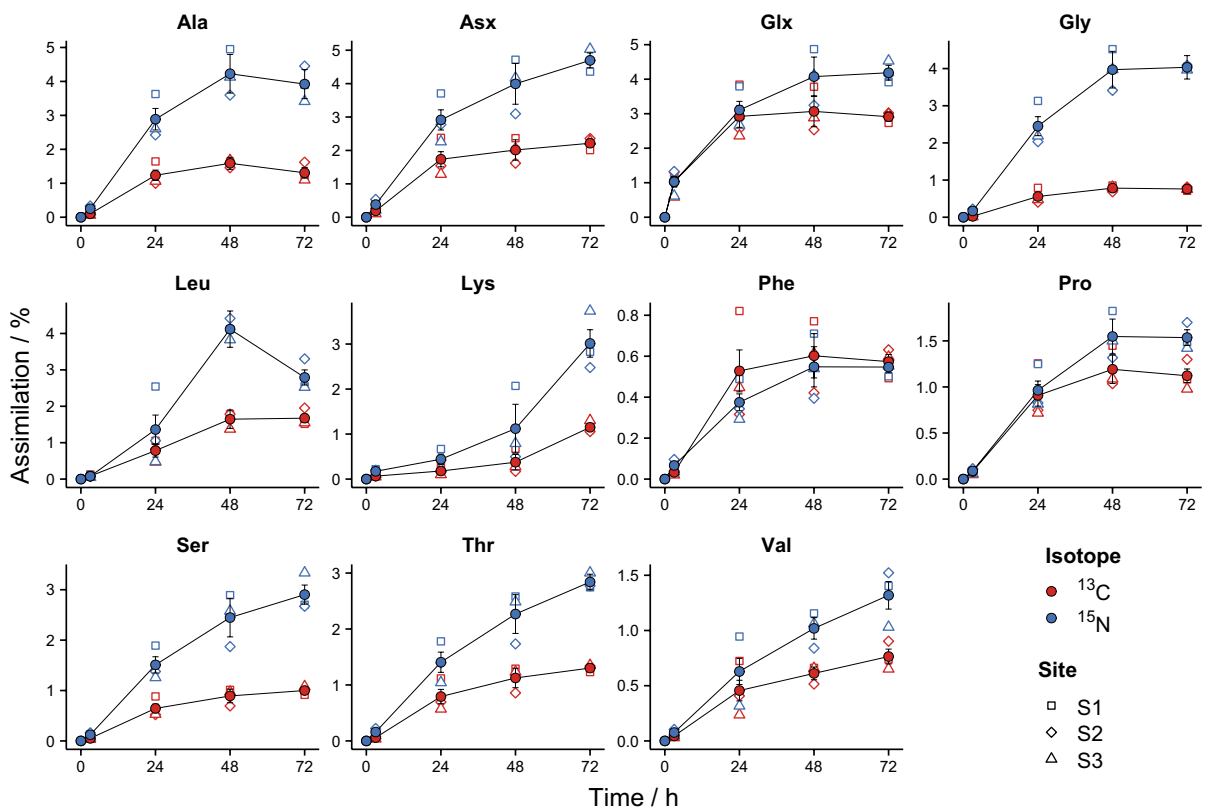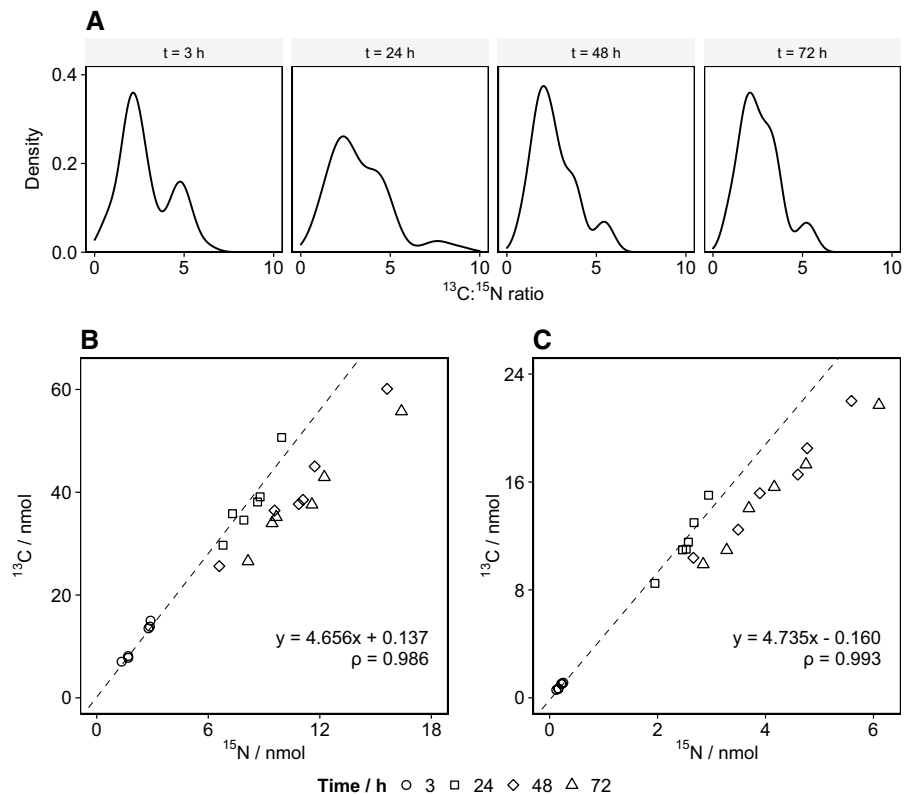

Fig. 2 Average percentage of assimilation of ^{13}C,^{15}N-Glu into individual proteinaceous AAs over time. Error bars show the *SE* ($n=6$)

Fig. 3 Density distribution of the $^{13}C:^{15}N$ ratio of individual proteinaceous AAs at different time points following the addition of $^{13}C,^{15}N$-Glu (**A**). Relationship of ^{13}C to ^{15}N over time for Glx (**B**) and Pro (**C**). Dash lines show regression models during the first 24 h of the experiment

On the other hand, the maximum C:N value of ~5 is close to the nominal C:N ratio of Glu. This confirmed that mostly all the $^{13}C,^{15}N$-Glu was transported directly into the microbial cells as proposed in section "THAAs concentration". To evaluate whether Glu is directly utilised for the biosynthesis of proteinaceous biomass, the C:N ratio of Glx and Pro were compared. The biosynthesis of Pro involves the reduction of the γ-carboxyl group of Glu to produce γ-glutamic semialdehyde, which spontaneously cyclises to L-Δ^1-pyrroline-5-carboxylate. This compound is then reduced to produce Pro (Csonka and Leisinger 2007; Fichman et al. 2015). In this pathway, the C:N ratio is conserved; therefore, it should be similar between the substrate (Glu) and the product (Pro). The ratios for both AAs were estimated using a regression model over the first 24 h of incubation (Fig. 3B and C) The concentrations of ^{13}C and ^{15}N were correlated for each AA during this period ($\rho > 0.986$, $P < 0.0001$). Estimated regression slopes were 4.656 ($SE = 0.321$) for

Glx, and 4.735 ($SE = 0.207$) for Pro. There was no evidence that the slopes were different between each other [$t(22) = 0.206$, $P = 0.8384$]. Similarly, there was no evidence that the individual slopes were different to the nominal C:N ratio of 5 [$t(11) = 1.072$, $P = 0.3066$ for Glx; t(11) = 1.283, $P = 0.2260$ for Pro]. This confirms the direct uptake and assimilation of AAs into microbial biomass in freshwaters.

^{15}N-NO$_3^-$ treatment

Specific assimilation rates (V, h^{-1}) for ^{15}N-NO$_3^-$ were considerably lower than ^{15}N-Glu (Table S2). This is because the assimilation of nitrate occurs via several biochemical reactions which are more energy demanding. Nitrate must be first reduced to nitrite and then to ammonium by nitrate and nitrite reductases, respectively (Stein and Klotz 2016; Zhang et al. 2020). Thereafter, either glutamate dehydrogenase or glutamine synthetase incorporate ammonium into biomass (Reitzer 2004). The highest average assimilation rates of ^{15}N-NO$_3^-$ were found in Phe and Glx.

Some AAs exhibited $\delta^{15}N$ values lower than the natural abundance after 3 h of incubation resulting in negative assimilation rates (Table S2). This was particularly apparent in Gly, Leu, Lys, Pro, Ser and Val at sampling site S3. Similar trends were seen by (Charteris et al. 2016) after the application of ^{15}N-NO_3^- to soil. Although the reason for this is unclear, the high energy requirements to assimilate nitrate could have led to the assimilation of energy-dense N-containing compounds depleted in ^{15}N. Transport rates (nmol g^{-1} h^{-1}) of Glx, Asx and Ala presented the highest average values which agree with the metabolic proximity and the observed transport rates for assimilation of ^{15}N-Glu.

The percentages of assimilation of ^{15}N-NO_3^- over time followed a different pattern compared to the ^{15}N-Glu treatment. The trends were characterised by a steady assimilation during the first 24 h, followed by an increase towards the end of the experiment (Fig. 4). The delay in the assimilation of ^{15}N-NO_3^-, as observed in Fig. 4, could be related to the

preferential assimilation of ammonium, due to higher energy costs, and the inhibition of ammonium over the uptake and assimilation of nitrate (Dortch 1990; Glibert et al. 2016). Highest assimilation was found in Asx ($M=0.45\%$, $SE=0.18$) and Glx ($M=0.42\%$, $SE=0.16$) whereas the lowest were present in Phe ($M=0.066\%$, $SE=0.026$) and Val ($M=0.134\%$, $SE=0.060$). Assimilation at site S1 was higher compared to the other sites.

Synthesis

The data presented here reveals pathways of carbon and nitrogen assimilation by particle-associated freshwater microbial communities. The rates and percentages of assimilation of each AA from the three study sites were combined and linked to the primarily biosynthetic pathways to compare the fluxes and connectivity of ^{13}C and ^{15}N processing (Fig. 5). For simplification, the percentages of assimilation were normalised to the amount of ^{15}N-Glu added, which
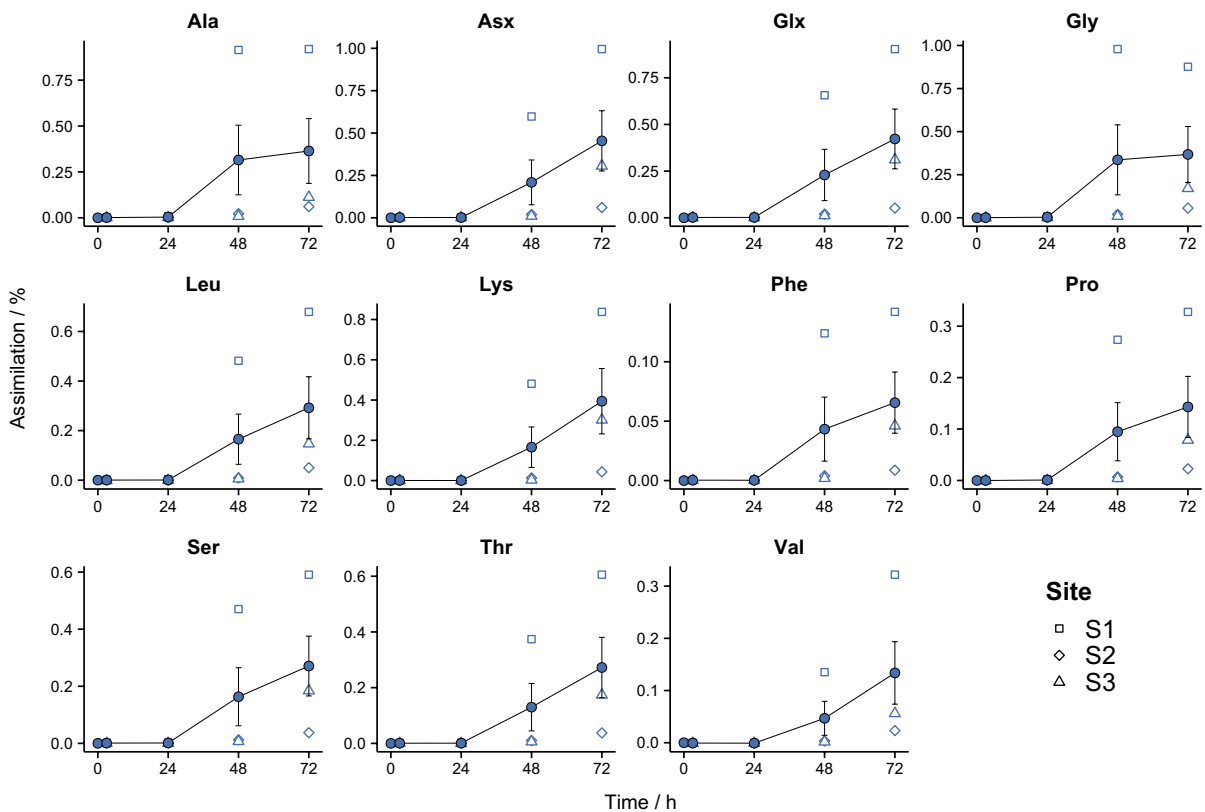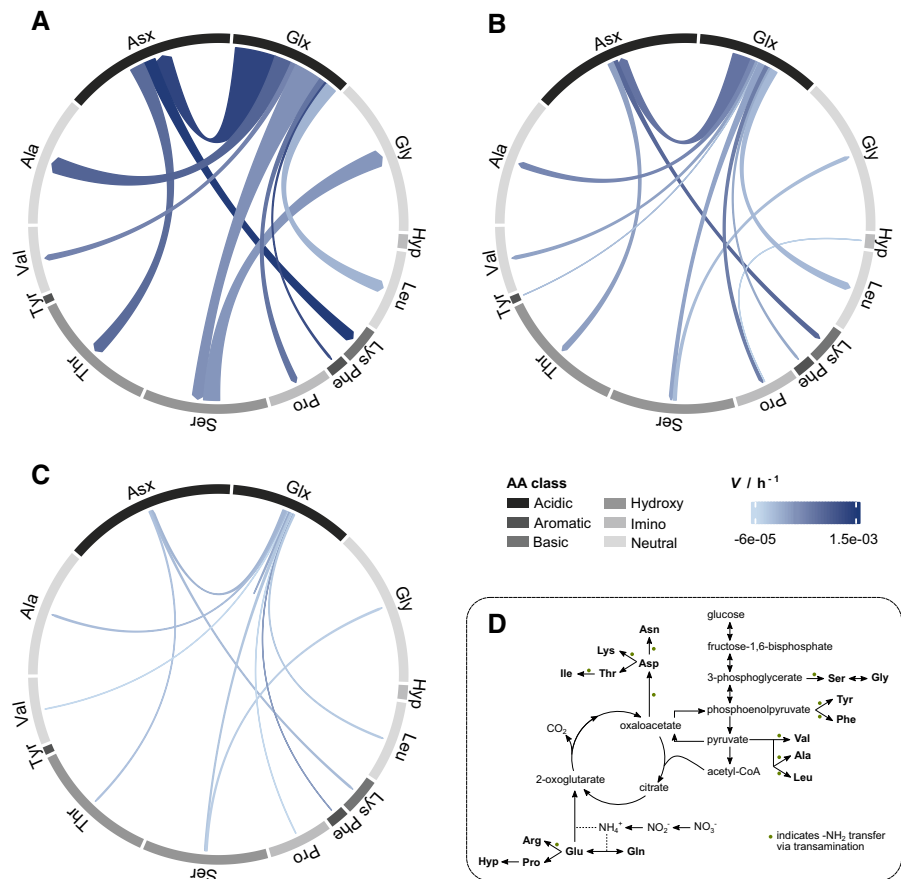

Fig. 4 Average percentage of assimilation of ^{15}N-NO_3^- into individual proteinaceous AAs over time. Error bars show the SE ($n=6$)

Fig. 5 Rates and percentages of assimilation of ^{15}N and ^{13}C from Glu (**A** and **B**, respectively) and ^{15}N from NO_3^- (**C**) into individual proteinaceous AAs. The circle represents the average composition of the pool of THAAs in mol %. The colour of the arrows represents the specific assimilation rates (V, h^{-1}) after 3 h, the width is proportional to the percentage of assimilation of the substrate after 72 h, and the direction represents the transfer of C or N according to the primary biosynthetic pathways of each AA (**D**)

was also scaled to represent the total pool of Glx. The diagrams show the average composition of the pool of THAAs in mol % (Fig. 5A, B and C). Secondary biosynthetic pathways were not included. The fluxes and biosynthetic links are useful to understand the metabolism of the complex consortia of microorganisms, associated with suspended particles, processing DOM and inorganic substrates in the water column. It must be noted that the rates of assimilation presented here should be interpreted with caution and not be considered 'real' rates. The concentration of suspended sediments added to the mesocosms exceeded the ambient concentration in the stream at the time of sampling but was below the global average (Müller et al. 2021). Moreover, the addition of ^{13}C,^{15}N-Glu at tracer level (< 10%) was not possible; but the amount added was not higher than 10% of the TN in the mesocosm. Nevertheless, it was shown that the addition of the substrates did not enhance microbial biomass production (section "THAAs concentration").

As previously discussed, there were differences in the total assimilation of ^{13}C-Glu and ^{15}N-Glu (^{15}N > ^{13}C) and a preference of ^{15}N from the organic versus the inorganic (^{15}N-Glu > ^{15}N-NO$_3^-$) substrate. Overall, the total microbial assimilation into newly synthesised proteinaceous biomass was estimated at 11.95% ($SE = 0.56$) and 27.60% ($SE = 1.10$) of ^{13}C and ^{15}N from Glu, respectively; and 3.18% ($SE = 1.30$) of ^{15}N from nitrate (Fig. 6A). Spatial differences in the total percentage of assimilation were also observed (Fig. 6B). There were likely higher percentages at site S2 and S3 for the ^{13}C,^{15}N-Glu treatment, and at site S1 for the ^{15}N-NO$_3^-$ treatment (Fig. 6B). These percentages were estimated after excluding the ^{13}C,^{15}N-Glu in excess and after 72 h of incubation. However, the maximum levels of assimilation were reached at different times at each site (Figs. 2 and 4); in particular, assimilation of ^{15}N-NO$_3^-$ did not reach a plateau before the end of the incubation.

Similar spatial differences were also observed in the assimilation and transport rates (Table S2 and
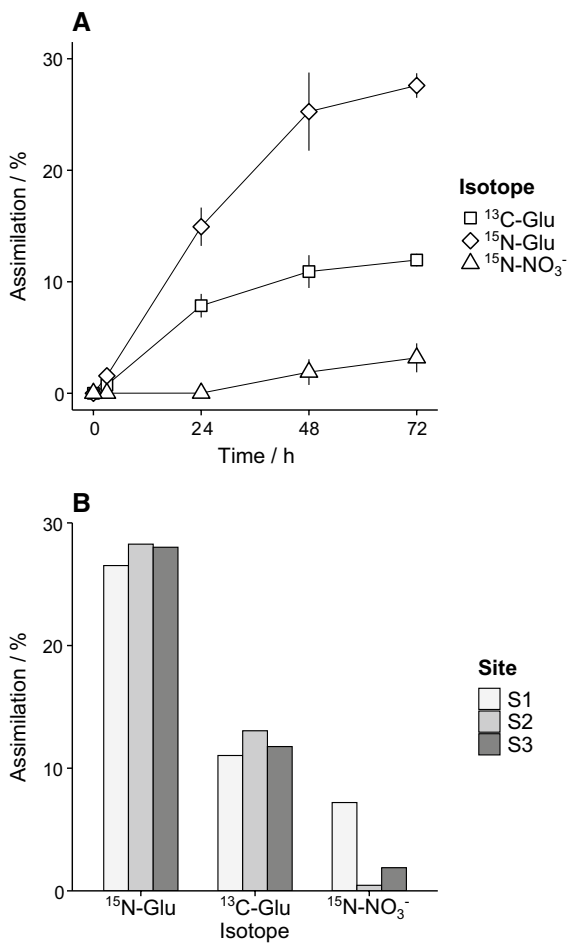
A

B

Fig. 6 Percentage of assimilation of ^{13}C and ^{15}N into the pool of THAAs over time (**A**), and the spatial differences in assimilation after 72 h (**B**). Error bars show the *SE* (*n*=6) (**A**)

S3). For the $^{13}C,^{15}N$-Glu treatment, assimilation rates were slightly higher at site S1 than S2, and lower at S2 than S3. In decreasing order, they followed sites S3 > S1 > S2. In contrast, transport rates were higher at site S2, probably due to the higher concentration of biomass, followed by sites S3 and S1. For the ^{15}N-NO_3^- treatment, a different trend was observed with higher assimilation and transport rates at site S2, followed by sites S1 and S3. These contrasts are based on cumulative values but not all the individual AAs followed the same trends. It was also observed that the decreasing order of the assimilation rates of individual AAs was different among sites suggesting distinctive processing of the substrates. In this regard, the experimental approach was affected by

restricted replication which hindered a robust spatial comparison of the fluxes and percentages of assimilation. Therefore, discussion of the metabolic pathways at each site is not included in this study. The trends of the percentages of assimilation over the course of experiment were also likely different (Figs. 2 and 4). There was a more rapid assimilation at site S1 during the first 24 h compared to the other two sites. This was particularly emphasised in the ^{15}N- NO_3^- treatment (Fig. 4). Such differences could be influenced by changes in the availability of nutrients at each site (i.e., ambient concentrations) as well as differences in microbial community composition (Middelburg and Nieuwenhuize 2000). For instance, the concentration of N-containing compounds (e.g., NH_4^+ and NO_3^-) increased downstream due to the STW outfall. Regarding the changes in the microbial composition, our approach does not allow direct links to be established between structure and functioning. However, it does provide evidence of the complexity of the population, and an overall representation (mechanistic and quantitative) of how the substrates are processed. Future efforts could be oriented to (a) the better understanding of the spatial and temporal differences in rates and fluxes of assimilation for each AA, and (b) the application of quantitative functional genomics in combination with SIP techniques.

Conclusions

The chemical and molecular characterisation of the suspended particles, in combination with the application of compound-specific SIP, provided insights into the role of suspended POM in freshwater nutrient cycling. In particular:

a. Regardless the proximity of the study sites, the composition of suspended sediments in the River Chew appeared to be distinct and highly influenced by the effluent of the STW.

b. Compound-specific isotope analysis of individual proteinaceous AAs allowed demonstration of assimilation of glutamate and nitrate into microbial biomass, showing the preference of the organic vs the inorganic substrate.

c. Specific assimilation and transport rates provided insights into the biochemical pathways by which

the substrates are assimilated by microbial communities. For instance, dual isotope analysis (^{13}C and ^{15}N) of Glx (glutamate and glutamine) and proline unequivocally confirmed the coupled assimilation of C and N into proteinaceous biomass.

d. The fluxes of assimilation of the substrates into the pool of THAAs varied spatially, which may be related to the distinct physical, chemical, and biological conditions at each site.

Our results highlight the value of SIP techniques to elucidate the fate of organic and inorganic compounds in freshwaters. This is particularly relevant for the better understanding of the molecular mechanisms regarding processing of low molecular weight DOM in freshwater ecosystems and the impacts of DOM and POM of differing molecular composition on the freshwater biota.

Declarations

References

Amalfitano S, Corno G, Eckert E et al (2017) Tracing particulate matter and associated microorganisms in freshwaters. Hydrobiologia 800:145–154. https://doi.org/10.1007/s10750-017-3260-x

Artifon V, Zanardi-Lamardo E, Fillmann G (2018) Aquatic organic matter: classification and interaction with organic microcontaminants. Sci Total Environ 649:1620–1635. https://doi.org/10.1016/j.scitotenv.2018.08.385

Attermeyer K, Catalán N, Einarsdottir K et al (2018) Organic carbon processing during transport through boreal inland waters: particles as important sites. J Geophys Res Biogeosci 123:2412–2428. https://doi.org/10.1029/2018jg004500

Aufdenkampe AK, Hedges JI, Richey JE et al (2001) Sorptive fractionation of dissolved organic nitrogen and amino acids onto fine sediments within the Amazon Basin. Limnol Oceanogr 46:1921–1935. https://doi.org/10.4319/lo.2001.46.8.1921

Berthelot H, Duhamel S, L'Helguen S et al (2019) NanoSIMS single cell analyses reveal the contrasting nitrogen sources for small phytoplankton. ISME J 13:651–662. https://doi.org/10.1038/s41396-018-0285-8

Brailsford FL, Glanville HC, Golyshin PN et al (2019) Nutrient enrichment induces a shift in dissolved organic carbon (DOC) metabolism in oligotrophic freshwater sediments. Sci Total Environ 690:1131–1139. https://doi.org/10.1016/j.scitotenv.2019.07.054

Brand WA, Assonov SS, Coplen TB (2010) Correction for the ^{17}O interference in δ^{13}C measurements when analyzing CO_2 with stable isotope mass spectrometry (IUPAC technical report). Pure Appl Chem 82:1719–1733. https://doi.org/10.1351/pac-rep-09-01-05

Bull ID, Parekh NR, Hall GH et al (2000) Detection and classification of atmospheric methane oxidizing bacteria in soil. Nature 405:175–178. https://doi.org/10.1038/35012061

Bunch ND, Bernot MJ (2012) Nitrate and ammonium uptake by natural stream sediment microbial communities in response to nutrient enrichment. Res Microbiol 163:137–141. https://doi.org/10.1016/j.resmic.2011.11.004

Burdon FJ, Bai Y, Reyes M et al (2020) Stream microbial communities and ecosystem functioning show complex responses to multiple stressors in wastewater. Glob Change Biol 26:6363–6382. https://doi.org/10.1111/gcb.15302

Callahan BJ, McMurdie PJ, Rosen MJ et al (2016) DADA2: high-resolution sample inference from illumina amplicon data. Nat Methods 13:581–583. https://doi.org/10.1038/nmeth.3869

Caspi R, Billington R, Keseler IM et al (2019) The MetaCyc database of metabolic pathways and enzymes—a 2019 update. Nucleic Acids Res 48:D445–D453. https://doi.org/10.1093/nar/gkz862

Charteris AF, Knowles TDJ, Michaelides K, Evershed RP (2016) Compound-specific amino acid ^{15}N stable isotope probing of nitrogen assimilation by the soil microbial biomass using gas chromatography/combustion/isotope ratio mass spectrometry. Rapid Commun Mass Sp 30:1846–1856. https://doi.org/10.1002/rcm.7612

Chen Y, Murrell JC (2010) When metagenomics meets stable-isotope probing: progress and perspectives. Trends Microbiol 18:157–163. https://doi.org/10.1016/j.tim.2010.02.002

Chonova T, Labanowski J, Cournoyer B et al (2018) River biofilm community changes related to pharmaceutical loads emitted by a wastewater treatment plant. Environ Sci Pollut R 25:9254–9264. https://doi.org/10.1007/s11356-017-0024-0

Conley M, Mojica M, Mohammed F et al (2017) Reaction of glycine with glyoxylate: competing transaminations, aldol reactions, and decarboxylations. J Phys Org Chem 30:e3709. https://doi.org/10.1002/poc.3709

Coplen TB (2011) Guidelines and recommended terms for expression of stable-isotope-ratio and gas-ratio measurement results. Rapid Commun Mass Spectrom 25:2538–2560. https://doi.org/10.1002/rcm.5129

Costanzo SD, Udy J, Longstaff B, Jones A (2005) Using nitrogen stable isotope ratios (δ^{15}N) of macroalgae to determine the effectiveness of sewage upgrades: changes in the extent of sewage plumes over four years in Moreton Bay, Australia. Mar Pollut Bull 51:212–217. https://doi.org/10.1016/j.marpolbul.2004.10.018

Cowie GL, Hedges JI (1994) Biochemical indicators of diagenetic alteration in natural organic matter mixtures. Nature 369:304–307. https://doi.org/10.1038/369304a0

Crump B, Baross J, Simenstad C (1998) Dominance of particle-attached bacteria in the Columbia River estuary, USA. Aquat Microb Ecol 14:7–18. https://doi.org/10.3354/ame014007

Csonka LN, Leisinger T (2007) Biosynthesis of proline. EcoSal Plus. https://doi.org/10.1128/ecosalplus.3.6.1.4

Dai J, Tang X, Gao G et al (2013) Effects of salinity and nutrients on sedimentary bacterial communities in oligosaline Lake Bosten, northwestern China. Aquat Microb Ecol 69:123–134. https://doi.org/10.3354/ame01627

Dauwe B, Middelburg JJ (1998) Amino acids and hexosamines as indicators of organic matter degradation state in North Sea sediments. Limnol Oceanogr 43:782–798. https://doi.org/10.4319/lo.1998.43.5.0782

Dekas AE, Parada AE, Mayali X et al (2019) Characterizing chemoautotrophy and heterotrophy in marine archaea and bacteria with single-cell multi-isotope NanoSIP. Front Microbiol 10:2682. https://doi.org/10.3389/fmicb.2019.02682

Docherty G, Jones V, Evershed RP (2001) Practical and theoretical considerations in the gas chromatography/combustion/isotope ratio mass spectrometry δ^{13}C analysis of small polyfunctional compounds. Rapid Commun Mass Spectrom 15:730–738. https://doi.org/10.1002/rcm.270

Dortch Q (1990) The interaction between ammonium and nitrate uptake in phytoplankton. Mar Ecol Prog Ser 61:183–201. https://doi.org/10.3354/meps061183

Drake TW, Raymond PA, Spencer RGM (2018) Terrestrial carbon inputs to inland waters: a current synthesis of estimates and uncertainty. Limnol Oceanogr Lett 3:132–142. https://doi.org/10.1002/lol2.10055

Drury B, Rosi-Marshall E, Kelly JJ (2013) Wastewater treatment effluent reduces the abundance and diversity of benthic bacterial communities in urban and suburban rivers. Appl Environ Microb 79:1897–1905. https://doi.org/10.1128/aem.03527-12

Du Y, Ramirez CE, Jaffé R (2018) Fractionation of dissolved organic matter by co-precipitation with iron: effects of composition. Environ Process 5:5–21. https://doi.org/10.1007/s40710-017-0281-4

Dugdale RC, Goering JJ (1967) Uptake of new and regenerated forms of nitrogen in primary productivity. Limnol Oceanogr 12:196–206. https://doi.org/10.4319/lo.1967.12.2.0196

Einarsdóttir K, Attermeyer K, Hawkes JA et al (2020) Particles and aeration at mire-stream interfaces cause selective removal and modification of dissolved organic matter. J Geophys Res Biogeosci. https://doi.org/10.1029/2020jg005654

Evans CD, Monteith DT, Cooper DM (2005) Long-term increases in surface water dissolved organic carbon: observations, possible causes and environmental impacts. Environ Pollut 137:55–71. https://doi.org/10.1016/j.envpol.2004.12.031

Evershed RP, Crossman ZM, Bull ID et al (2006) ^{13}C-Labelling of lipids to investigate microbial communities in the environment. Curr Opin Biotech 17:72–82. https://doi.org/10.1016/j.copbio.2006.01.003

Feehily C, Karatzas KAG (2013) Role of glutamate metabolism in bacterial responses towards acid and other stresses. J Appl Microbiol 114:11–24. https://doi.org/10.1111/j.1365-2672.2012.05434.x

Fernandes D, Wu Y, Shirodkar PV et al (2019) Spatial and temporal variations in source, diagenesis, and fate of organic matter in sediments of the Netravati River, India. Hydrol Process 33:2642–2657. https://doi.org/10.1002/hyp.13516

Fernandes D, Wu Y, Shirodkar PV et al (2020) Sources and preservation dynamics of organic matter in surface sediments of Narmada River, India—illustrated by amino acids. J Mar Syst 201:103239. https://doi.org/10.1016/j.jmarsys.2019.103239

Fichman Y, Gerdes SY, Kovács H et al (2015) Evolution of proline biosynthesis: enzymology, bioinformatics, genetics, and transcriptional regulation. Biol Rev 90:1065–1099. https://doi.org/10.1111/brv.12146

Glibert PM, Wilkerson FP, Dugdale RC et al (2016) Pluses and minuses of ammonium and nitrate uptake and assimilation by phytoplankton and implications for productivity and community composition, with emphasis on nitrogen-enriched conditions. Limnol Oceanogr 61:165–197. https://doi.org/10.1002/lno.10203

Glibert PM, Middelburg JJ, McClelland JW, Zanden MJV (2019) Stable isotope tracers: enriching our perspectives and questions on sources, fates, rates, and pathways of major elements in aquatic systems. Limnol Oceanogr 64:950–981. https://doi.org/10.1002/lno.11087

Glibert PM, Heil CA, Madden CJ, Kelly SP (2021) Dissolved organic nutrients at the interface of fresh and marine waters: flow regime changes, biogeochemical cascades and picocyanobacterial blooms—the example of Florida Bay, USA. Biogeochemistry. https://doi.org/10.1007/s10533-021-00760-4

Groeneveld M, Catalán N, Attermeyer K et al (2020) Selective adsorption of terrestrial dissolved organic matter to inorganic surfaces along a boreal inland water continuum. J Geophys Res Biogeosci. https://doi.org/10.1029/2019jg005236

Gupta LP, Subramanian V, Ittekkot V (1997) Biogeochemistry of particulate organic matter transported by the Godavari River, India. Biogeochemistry 38:103–128. https://doi.org/10.1023/a:1005732519216

Gweon HS, Bowes MJ, Moorhouse HL et al (2021) Contrasting community assembly processes structure lotic bacteria metacommunities along the river continuum. Environ Microbiol 23:484–498. https://doi.org/10.1111/1462-2920.15337

Hagberg A, Gupta S, Rzhepishevska O et al (2021) Do environmental pharmaceuticals affect the composition of bacterial communities in a freshwater stream? A case study of the Knivsta river in the south of Sweden. Sci Total Environ 763:142991. https://doi.org/10.1016/j.scitotenv.2020.142991

He W, Chen M, Schlautman MA, Hur J (2016) Dynamic exchanges between DOM and POM pools in coastal and inland aquatic ecosystems: a review. Sci Total Environ 551:415–428. https://doi.org/10.1016/j.scitotenv.2016.02.031

Hunter WR, Niederdorfer R, Gernand A et al (2016) Metabolism of mineral-sorbed organic matter and microbial lifestyles in fluvial ecosystems. Geophys Res Lett 43:1582–1588. https://doi.org/10.1002/2016gl067719

Jia Z, Liu T, Xia X, Xia N (2016) Effect of particle size and composition of suspended sediment on denitrification in river water. Sci Total Environ 541:934–940. https://doi.org/10.1016/j.scitotenv.2015.10.012

Junk G, Svec HJ (1958) The absolute abundance of the nitrogen isotopes in the atmosphere and compressed gas from various sources. Geochim Cosmochim Acta 14:234–243. https://doi.org/10.1016/0016-7037(58)90082-6

Kerner M, Hohenberg H, Ertl S et al (2003) Self-organization of dissolved organic matter to micelle-like microparticles in river water. Nature 422:150–154. https://doi.org/10.1038/nature01469

Knowles TDJ, Chadwick DR, Bol R, Evershed RP (2010) Tracing the rate and extent of N and C flow from ^{13}C,^{15}N-glycine and glutamate into individual de novo synthesised soil amino acids. Org Geochem 41:1259–1268. https://doi.org/10.1016/j.orggeochem.2010.09.003

Lu Y, Bauer JE, Canuel EA et al (2013) Photochemical and microbial alteration of dissolved organic matter in temperate headwater streams associated with different land use. J Geophys Res Biogeosci 118:566–580. https://doi.org/10.1002/jgrg.20048

Mackay EB, Feuchtmayr H, Ville MMD et al (2020) Dissolved organic nutrient uptake by riverine phytoplankton varies along a gradient of nutrient enrichment. Sci Total Environ 722:137837. https://doi.org/10.1016/j.scitotenv.2020.137837

Manefield M, Whiteley AS, Griffiths RI, Bailey MJ (2002) RNA stable isotope probing, a novel means of linking microbial community function to phylogeny. Appl Environ Microb 68:5367–5373. https://doi.org/10.1128/aem.68.11.5367-5373.2002

Mansour I, Heppell CM, Ryo M, Rillig MC (2018) Application of the microbial community coalescence concept to riverine networks. Biol Rev 93:1832–1845. https://doi.org/10.1111/brv.12422

Martin M (2011) Cutadapt removes adapter sequences from high-throughput sequencing reads. Embnet J 17:10–12. https://doi.org/10.14806/ej.17.1.200

Mayer LM, Schick LL, Skorko K, Boss E (2006) Photodissolution of particulate organic matter from sediments. Limnol Oceanogr 51:1064–1071. https://doi.org/10.4319/lo.2006.51.2.1064

Meija J, Coplen TB, Berglund M et al (2016) Isotopic compositions of the elements 2013 (IUPAC technical report). Pure Appl Chem 88:293–306. https://doi.org/10.1515/pac-2015-0503

Middelburg J, Nieuwenhuize J (2000) Nitrogen uptake by heterotrophic bacteria and phytoplankton in the nitrate-rich Thames estuary. Mar Ecol Prog Ser 203:13–21. https://doi.org/10.3354/meps203013

Miflin BJ, Habash DZ (2002) The role of glutamine synthetase and glutamate dehydrogenase in nitrogen assimilation and possibilities for improvement in the nitrogen utilization of crops. J Exp Bot 53:979–987. https://doi.org/10.1093/jexbot/53.370.979

Monteith DT, Stoddard JL, Evans CD et al (2007) Dissolved organic carbon trends resulting from changes in atmospheric deposition chemistry. Nature 450:537–540. https://doi.org/10.1038/nature06316

Morgan M, Anders S, Lawrence M et al (2009) ShortRead: a bioconductor package for input, quality assessment and exploration of high-throughput sequence data. Bioinformatics 25:2607–2608. https://doi.org/10.1093/bioinformatics/btp450

Müller G, Middelburg JJ, Sluijs A (2021) Introducing GloRiSe—a global database on river sediment composition. Earth Syst Sci Data 13:3565–3575. https://doi.org/10.5194/essd-13-3565-2021

Nemergut DR, Schmidt SK, Fukami T et al (2013) Patterns and processes of microbial community assembly. Microbiol Mol Biol R 77:342–356. https://doi.org/10.1128/mmbr.00051-12

Noacco V, Duffy CJ, Wagener T et al (2019) Drivers of inter-annual and intra-annual variability of dissolved organic carbon concentration in the River Thames between 1884 and 2013. Hydrol Process 33:994–1012. https://doi.org/10.1002/hyp.13379

Pagès H, Aboyoun P, Gentleman R, DebRoy S (2021). Biostrings: efficient manipulation of biological strings.

R package version 2.60.1, https://bioconductor.org/packages/Biostrings. Accessed 01 June 2021

Pemberton JA, Lloyd CEM, Arthur CJ et al (2020) Untargeted characterisation of dissolved organic matter contributions to rivers from anthropogenic point sources using direct-infusion and high-performance liquid chromatography/Orbitrap mass spectrometry. Rapid Commun Mass Spectrom. https://doi.org/10.1002/rcm.8618

Phillips JM, Russell MA, Walling DE (2000) Time-integrated sampling of fluvial suspended sediment: a simple methodology for small catchments. Hydrol Process 14:2589–2602. https://doi.org/10.1002/1099-1085(20001015)14:14%3c2589::aid-hyp94%3e3.3.co;2-4

Pinheiro J, Bates D, DebRoy S, Sarkar D, R Core Team (2021). nlme: Linear and nonlinear mixed effects models. R package version 3.1–148, https://CRAN.R-project.org/package=nlme. Accessed 01 June 2021

Quast C, Pruesse E, Yilmaz P et al (2013) The SILVA ribosomal RNA gene database project: improved data processing and web-based tools. Nucleic Acids Res 41:D590–D596. https://doi.org/10.1093/nar/gks1219

R Core Team (2021). R: a language and environment for statistical computing. R Foundation for Statistical Computing, Vienna, Austria. URL https://www.R-project.org/

Reay MK, Charteris AF, Jones DL, Evershed RP (2019) ^{15}N-amino sugar stable isotope probing (^{15}N-SIP) to trace the assimilation of fertiliser-N by soil bacterial and fungal communities. Soil Biol Biochem 138:107599. https://doi.org/10.1016/j.soilbio.2019.107599

Regnier P, Friedlingstein P, Ciais P et al (2013) Anthropogenic perturbation of the carbon fluxes from land to ocean. Nat Geosci 6:597–607. https://doi.org/10.1038/ngeo1830

Reitzer L (2004) Biosynthesis of glutamate, aspartate, asparagine, L-alanine, and D-alanine. EcoSal Plus. https://doi.org/10.1128/ecosalplus.3.6.1.3

Sánchez-Carrillo S, Álvarez-Cobelas M (2018) Stable isotopes as tracers in aquatic ecosystems. Environ Rev 26:69–81. https://doi.org/10.1139/er-2017-0040

Simon M, Grossart H, Schweitzer B, Ploug H (2002) Microbial ecology of organic aggregates in aquatic ecosystems. Aquat Microb Ecol 28:175–211. https://doi.org/10.3354/ame028175

Smith MW, Allen LZ, Allen AE et al (2013) Contrasting genomic properties of free-living and particle-attached microbial assemblages within a coastal ecosystem. Front Microbiol 4:120. https://doi.org/10.3389/fmicb.2013.00120

Stauffer GV (2004) Regulation of serine, glycine, and one-carbon biosynthesis. EcoSal Plus. https://doi.org/10.1128/ecosalplus.3.6.1.2

Steffy LY, Kilham SS (2004) Elevated δ^{15}n in stream biota in areas with septic tank systems in an urban watershed. Ecol Appl 14:637–641. https://doi.org/10.1890/03-5148

Stein LY, Klotz MG (2016) The nitrogen cycle. Curr Biol 26:R94–R98. https://doi.org/10.1016/j.cub.2015.12.021

Veuger B, Middelburg JJ, Boschker HTS, Houtekamer M (2005) Analysis of 15N incorporation into D-alanine: a new method for tracing nitrogen uptake by bacteria. Limnol Oceanogr Methods 3:230–240. https://doi.org/10.4319/lom.2005.3.230

Walters W, Hyde ER, Berg-Lyons D et al (2016) Improved bacterial 16S rRNA gene (V4 and V4–5) and fungal internal transcribed spacer marker gene primers for microbial community surveys. Msystems 1:e00009-15. https://doi.org/10.1128/msystems.00009-15

Wang Y, Huang WE, Cui L, Wagner M (2016) Single cell stable isotope probing in microbiology using Raman microspectroscopy. Curr Opin Biotech 41:34–42. https://doi.org/10.1016/j.copbio.2016.04.018

Wang L, Zhang J, Li H et al (2018) Shift in the microbial community composition of surface water and sediment along an urban river. Sci Total Environ 627:600–612. https://doi.org/10.1016/j.scitotenv.2018.01.203

Wu L, Ning D, Zhang B et al (2019) Global diversity and biogeography of bacterial communities in wastewater treatment plants. Nat Microbiol 4:1183–1195. https://doi.org/10.1038/s41564-019-0426-5

Xia X, Liu T, Yang Z et al (2017) Enhanced nitrogen loss from rivers through coupled nitrification-denitrification caused by suspended sediment. Sci Total Environ 579:47–59. https://doi.org/10.1016/j.scitotenv.2016.10.181

Yamashita Y, Jaffé R (2008) Characterizing the interactions between trace metals and dissolved organic matter using excitation−emission matrix and parallel factor analysis. Environ Sci Technol 42:7374–7379. https://doi.org/10.1021/es801357h

Yates CA, Johnes PJ, Spencer RGM (2019) Characterisation of treated effluent from four commonly employed wastewater treatment facilities: a UK case study. J Environ Manag 232:919–927. https://doi.org/10.1016/j.jenvman.2018.12.006

Yoshimura C, Fujii M, Omura T, Tockner K (2010) Instream release of dissolved organic matter from coarse and fine particulate organic matter of different origins. Biogeochemistry 100:151–165. https://doi.org/10.1007/s10533-010-9412-y

Zeglin LH (2015) Stream microbial diversity in response to environmental changes: review and synthesis of existing research. Front Microbiol 6:454. https://doi.org/10.3389/fmicb.2015.00454

Zhang X, Ward BB, Sigman DM (2020) Global nitrogen cycle: critical enzymes, organisms, and processes for nitrogen budgets and dynamics. Chem Rev 120:5308–5351. https://doi.org/10.1021/acs.chemrev.9b00613

Publisher's Note Springer Nature remains neutral with regard to jurisdictional claims in published maps and institutional affiliations.